ChemComm

COMMUNICATION

View Article Online
View Journal | View Issue

Cite this: *Chem. Commun.*, 2019, **55**, 8238

Received 14th May 2019,
Accepted 20th June 2019

DOI: 10.1039/c9cc03714d

rsc.li/chemcomm

Deciphering the origin of variation in the spin ground state and oxidation state of a {Mn_{19}} cluster on a Au(111) surface: is the Au(111) surface innocent?†

Rizwan Nabi and Gopalan Rajaraman *

Periodic DFT calculations on a {Mn_{19}} cluster possessing S = 83/2 ground state and its reduced variant on a Au(111) surface unravel the importance of structural distortions that triggered drastic variations in the J values leading to a large reduction in the spin ground state. Reduction of Mn^{III} ions leads to antiferromagnetic Js with a very small spin ground state manifesting the non-innocent behavior of the Au(111) surface.

Single molecule magnets offer an attractive avenue for miniaturization of storage devices and have potential applications in spintronics and quantum computing.[1] There are several hurdles in realizing the potential applications of these molecules.[2] Among all, controlling their magnetic properties upon adsorption remains a significant challenge. This is evident from the fact that numerous transition metal and lanthanide complexes that are reported to possess very large blocking temperatures, often lose their magnetic characteristics upon adsorption on surfaces.[3] In this regard, the observation of hysteresis of functionalized {Fe_4}[4] molecules on Au(111) has gained attention as this study suggests that the microscopic properties, such as quantum tunneling of magnetization, of molecular magnets are observable upon adsorption. In lanthanide-based SMMs, the blocking temperatures are raised to as high as 80 K;[5] however, their practical utility remains elusive unless such effects are demonstrated on surfaces.[6,7]

As surface deposition remains the primary way to address the molecule for a possible read-out, it is crucial to understand how the properties/structure of the molecule alter upon adsorption. Computational tools are indispensable in this regard, as they offer the structure of molecules on surfaces and yield insights into their magnetic properties.[8] It is important to mention here that the archetypal {Mn_{12}} upon adsorption on Au(111), lost its SMM characteristics while a {Mn_6} cluster possessing the S = 12 ground state retains them.[9] This clearly suggests that the properties of molecules on surfaces are difficult to comprehend and the structure of the molecule adsorbed on the surface might pave the way forward. Among the manganese clusters, it is worth mentioning here about the $[Mn^{III}_{12}Mn^{II}_7(\mu_4\text{-}O)_8(\mu_3\text{-}N_3)_8(HL)_{12}(MeCN)_6]Cl_2$·(**1**; H_3L = 2,6-bis(hydroxy-methyl)-4-methylphenol; Mn_{19} here onwards) cluster reported to possess a record high-spin ground state of S = 83/2 for a transition metal complex for a long time.[10] Another variant of this {Mn_{19}} cluster exhibits a ground state of S = 73/2.[11] Recently, the thiol functionalized variant of {Mn_{19}SMe} ($[Mn^{III}_{12}Mn^{II}_7(\mu_4\text{-}O)_8(\mu_3\text{-}Cl)_{7.7}(\mu_3\text{-}Me)_{0.3}(HLSMe)_{12}(MeOH)_6]Cl_2$·($H_3$LSMe = 2,6-bis(hydroxy-methyl)-4-mercaptomethylphenol; **1**) has been synthesized and has been deposited on a Au(111) surface. While scanning tunneling microscopy (STM) images indicate that the molecules are intact, the X-ray absorption spectroscopy (XAS) and X-ray magnetic circular dichroism (XMCD) studies suggest a reduction of Mn^{III} to Mn^{II} at lower concentrations.[12] Deposition of this molecule on a highly oriented pyrolytic graphene (HOPG) surface reveals that the molecules are intact and no reduction has been observed.[12]

In this work, we aim to model the structure of Mn_{19}SMe on a Au(111) surface to estimate the exchange coupling constant for this cluster upon adsorption. Moreover, as the molecule is large, various possible orientations of **1** on Au(111) have been postulated, and we aim to determine the energetically stable orientation and how this orientation alters the magnetic properties of the cluster upon adsorption? As earlier experimental evidence clearly reveals that the Mn^{III} ions are reduced to Mn^{II} ions upon adsorption, we probe the binding affinity of such a reduced cluster, and its magnetic properties and redox potential that led to such spontaneous reduction. The structure of **1** (Fig. 1a) consists of twelve Mn^{III} ions and seven Mn^{II} ions connected *via* a μ_4-oxo bridge, and μ_3-Cl and μ_2-OMe bridges. The twelve Mn^{III} atoms form two octahedra, which are connected by Mn^{II} tetrahedra with a common Mn^{II} vertex. The magnetic studies suggest that complex **1** possess the S = 83/2 ground state arising from ferromagnetic coupling among all the Mn ions.

To assess the ground state of **1**, we have undertaken DFT calculations to estimate the exchange coupling constants employing the PBE functional including dispersion corrections. The J values obtained from the PBE functional reproduce the sign of J in all cases, though the magnitude of Js are slightly overestimated. Overall the estimated Js are in agreement with the ones obtained using the

Department of Chemistry, Indian Institute of Technology Bombay, Powai, Mumbai 400076, India. E-mail: rajaraman@chem.iitb.ac.in

† Electronic supplementary information (ESI) available: Computational methodology employed, computed structural and spin density plots. See DOI: 10.1039/c9cc03714d

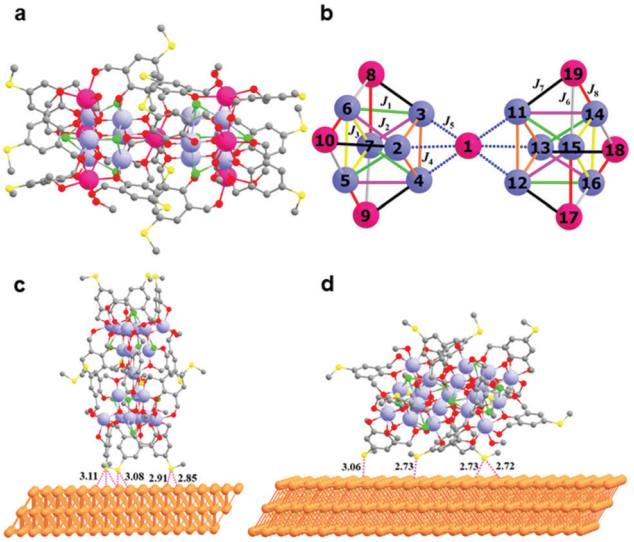

Fig. 1 (a) X-ray structure of complex **1**. (b) Schematic representation of the various exchange interactions present in **1**. (c) End-on orientation of **1** on Au(111). (d) The side-on orientation of **1** on Au(111). Colour code: Mn^{II} – pink, Mn^{III} – purple, O – red, Cl – green; S – yellow, C – grey and Au – golden yellow.

hybrid B3LYP functional[10c] offering confidence in the methodology employed. For a detailed discussion of the computational methodology and for the suitability of the chosen functional employed and the corresponding exchange Hamiltonian see Table S1, ESI.†

There are eight different exchange-coupling constants present in **1** (Fig. 1b) and these have been classified based on the oxidation state of the Mn centers and the nature of the bridging ligands. Here, J_1–J_4 describe interactions within the $\{Mn^{III}\cdots Mn^{III}\}$ pairs (see Table 1).

Here, four different *J*s are required taking into consideration the symmetry and difference in the associated structural parameters such as Mn–O and Mn–Cl distances, and Mn–O–Mn angles (see Tables S2–S5, ESI†). The J_5 describes interactions between the central Mn^{II} ion and the next-nearest Mn^{III} ions while J_6–J_8 describe the interactions between the apical Mn^{II} ions to the Mn^{III} ions (see Fig. 1b). The exchange topology adapted here is the same as the one adopted earlier, and the chosen methodology has been shown to yield good numerical estimates of the *J* values.[10c] Calculations were performed employing eight different broken symmetry solutions (see ESI† for further details and Fig. S2–S4 for the spin density plots).

The estimated J_1–J_8 values for the X-ray structure of **1** are given in Table 1 ($J_{X\text{-ray}}$). The J_1–J_8 values estimated for complex **1** are ferromagnetic in nature and are very similar to the values obtained for the original Mn_{19} cluster.[10c] This set of *J* values leads to the ground state of $S = 83/2$ and this is in agreement with the experimental findings.[12a] Although all the computed *J*s are ferromagnetic, there are some shifts in the absolute values of *J*s that need to be discussed. In particular, the J_4 interactions are estimated to be +0.9 cm^{-1} for **1** compared to 22.2 cm^{-1} estimated for the original structure.[10c] This is correlated to the fact that the μ_3-N_3 bridges in Mn_{19} are replaced by μ_3-Cl in complex **1** and this has led to a variation in the Mn–X–Mn angles ($X = N_3^-$, Cl^-) leading to an alteration in *J*s. Furthermore, the structural parameter around J_4 interactions suggests a large change in Mn–Cl–Mn and Mn–O–Mn angles leading to a smaller *J* value.

Table 1 PBE estimated *J* for **1** using various geometries

Exchange coupling	Bridging ligands	$J_{X\text{-ray}}$	$J_{end\text{-}on}$	$J_{side\text{-}on}$	$J_{red.}$
J_1	μ_4-O, μ_3-Cl	9.8	−5.4	7.5	29.3
J_2	μ_4-O, μ_3-Cl	17.9	27.8	25.5	−117.4
J_3	μ_4-O, μ_3-Cl	29.7	101.9	58.5	−31.0
J_4	μ_4-O, μ_3-Cl	0.9	−78.8	−35	−45.4
J_5	μ_4-O, μ_2-O	1.6	5	−1.1	−47.8
J_6	μ_4-O, μ_2-O	7.6	2.7	9.2	−23.9
J_7	μ_4-O, μ_2-O	4.8	−1.9	3.8	−8.29
J_8	μ_4-O, μ_2-O	0.6	−3.9	0.6	−32.2

In the next step, we have optimized the crystal structure of the pristine cluster on the Au(111) surface employing periodic boundary conditions. Earlier experimental and theoretical reports on the adsorption of thiols on Au(111) revealed that the terminal S–H/Me group upon adsorption on the surface cleaves leading to the formation of $RS^{\bullet}$ type species which tend to bind to the surface strongly.[13] To ascertain if such scenarios are possible here, we have estimated the binding energy for the S–Me dissociated and undissociated Mn_{19} species on Au(111). Additionally, there are two possible orientations of **1** on Au(111) and these are (a) end-on orientation with the C_3-axis of the molecule parallel to the Au(111) surface normal and (b) side-on orientation with the C_3-axis of the molecule perpendicular to the surface normal of Au(111) (Fig. 1c and d). Considering both the possibilities, our calculations energetically favour un-dissociated Mn_{19}SMe adsorption for both side-on and end-on orientations (end-on: −361.5 kJ mol^{-1} *vs.* +252.3 kJ mol^{-1}; side-on: −514 kJ mol^{-1} *vs.* +227.2 kJ mol^{-1}). Between the two orientations, clearly, side-on orientation of the Mn_{19}SMe (**1**) is favoured energetically, however stronger binding of the end-on orientation suggests that if the molecule approaches the surface in an end-on fashion, this is likely to stay in this orientation leading to a mixture of both possibilities being present on the Au(111) surface. This is in agreement with the experimental findings.

The estimated *J* values for the two orientations are given in Table 1. It is important to note here that two such orientations of the $\{Mn_{19}\}$ cluster on the HOPG surface were noted earlier.[12] Calculations reveal a substantial change in both sign and magnitude of the *J*s for both orientations ($J_{end\text{-}on}$, $J_{side\text{-}on}$). The $\{Mn^{III}\cdots Mn^{III}\}$ J_1–J_4 interactions are found to alter significantly for both sets. The J_1 interaction is found to be antiferromagnetic for the end-on geometry while it is only perturbed for the side-on geometries. Close inspection of the structural parameters reveals significant changes to the Mn–O–Mn angles with an average angle of 118.5°, 111.8°, and 115.0° for X-ray, end-on and side-on geometries, respectively. As per the magneto-structural correlation developed earlier on the dinuclear building units, smaller Mn^{III}–O–Mn^{III} angle enhances the antiferromagnetic part of the exchange leading to a switch in the sign of magnetic exchange for the end-on geometry, while the sign is retained for the side-on geometry. This is nicely reflected in the estimated bond angles. For J_2 interactions, the magnitude of ferromagnetic interaction was found to increase as we go from X-ray to side-on and end-on structures. As this is correlated to the same triangle, here the concomitant Mn^{III}–O–Mn^{III} angles are found to increase upon adsorption (114.3°, 117.5°, and 116.8° for X-ray,

end-on and side-on structures, respectively) leading to stronger ferromagnetic coupling. Similarly, for both geometries, the J_3 interactions are found to be strongly ferromagnetic (as the JT axes are perpendicular leading to type-III classification[14]), overriding all other interactions and this is essentially due to alteration in the angles and the Mn–O distances. J_4: this interaction has significantly altered upon adsorption. Both in the side-on and end-on geometries, this interaction is strongly antiferromagnetic compared to weak ferromagnetic coupling observed in the X-ray structure. While the Mn^{III}–O–Mn^{III} angles are altered slightly, it cannot explain the drastic variations in the *J*s. A closer look at the structure reveals that the μ_3-Cl bridges are distorted strongly leading to a very long $Mn^{III}\cdots$Cl bond distance (from 2.66 in X-ray to 3.06 Å in end-on geometries) suggesting the formation of five-coordinate Mn^{III} atoms with J_4-mediated primarily *via* μ_4-O bridges. While this is the case for the end-on geometries, for side-on geometries the $Mn^{III}\cdots$Cl elongations are only moderate (2.84 Å, see Fig. 2a–c), leaving stronger exchange to be mediated by the μ_4-O bridge and also *via* μ_3-Cl, leading to a relatively weaker antiferromagnetic coupling (-35.0 cm^{-1} *vs.* -78.8 cm^{-1}, see Table 1).

The J_5 interaction is very important as this connects two supertetrahedral {Mn9} units. This has been treated globally on par with other *J*s. Importantly the role of Mn$\cdots$Mn distances in the nature of J_5 has been established earlier by Ruiz *et al.*, and later on the same has been verified by replacing other metal ions in place of the central Mn(II).[10c] In connection with this, this interaction plays a crucial role in determining the ground state *S* value of this cluster. The J_5 interaction in this cluster is mediated *via* a weak μ_4-O and μ_2-O(R) group. As we move from the side-on to end-on structure, the *J* varies from weak ferromagnetic coupling to moderate antiferromagnetic coupling. While the μ_4-O Mn^{II}–O–Mn^{III} angles are found to be similar, the μ_2-O(alkoxo) Mn^{II}–O–Mn^{III} angles are altered where a large angle tends to enhance the antiferromagnetic part of the exchange, rationalizing the computed *J*s (111.2°, 107.6°, 114.1° for X-ray, end-on, and side-on, respectively). For J_6–J_8 coupling, only minor alterations are seen in the magnitude for the side-on geometries while for the end-on geometries, the signs of J_7 and J_8 are switched to antiferromagnetic coupling. This switch of the sign is important as this dictates the ground state *S* value for the overall cluster. For the end-on geometry, one of the Mn^{II}–O–Mn^{III} angles is found to be significantly larger compared to the others and this leads to a switch in the sign of the J_7 and J_8 interactions (J_7: 103.1° *vs.* 107.8°; J_8 104.6° *vs.* 105.4°, see Tables S2–S4 in ESI†).

It is important to note here that the J_6–J_8 interactions are significantly altered only in the end-on structures while this is not the case for the side-on geometry. This is mainly due to the fact that in the side-on arrangements, the S–Me group located closer to the central Mn^{II} ions are binding to the Au(111) surface with the terminal S–Me exhibiting weak or no interactions. This leads to less distortion on the peripheral Mn^{II} ions and hence the related *J*s are only marginally altered. For the end-on structures, on the other hand, the three terminal S–Me groups bind strongly to the Au(111), leading to a greater degree of distortion on the apical Mn^{II} atoms leading to a switch in the sign of the *J* values. Due to these variations, different ground *S* values are expected for these two geometries. As the system size is very large, it is not possible to perform a full diagonalization of the exchange Hamiltonian using the estimated *J* values to determine the ground state *S* value for this cluster. As there are no competing interactions, we have constructed various smaller models of the $\{Mn_{19}\}$ cluster (see ESI† for details) and one can arrive at the following information about the spin ground state of both the side-on and end-on geometries: (i) since the J_4 interactions are strongly antiferromagnetic, the $\{Mn^{III}\}$ triangles (Mn2–Mn3–Mn4/Mn11–Mn12–Mn13) involved with J_4 exhibit spin frustration leading to an $S = 0$ ground state. This ground state *S* value is barely influenced by other *J*s as J_4 is very strong. (ii) Similarly, the $\{Mn^{III}\}$ triangles (Mn5–Mn6–Mn7/Mn14–Mn15–Mn16) connected *via* the J_3 interaction are strongly ferromagnetic leading to an $S = 6$ ground state for these triangular units and this ground state is also barely influenced by other *J*s. Thus, the ground state *S* values are controlled by the peripheral interaction with the Mn^{2+} ions. Our model calculations with the computed *J* suggest possible ground state *S* value of 11/2 (see Fig. 2d for a tentative orientation of the ground spin configuration) for the end-on and $S = 59/2$ for the side-on geometries (see Fig. S5 in ESI† for the ground state spin configuration). For the end-on geometry, a drastic reduction compared to the X-ray structure is noted while for the side-on geometry only a moderate reduction in the *S* value is noted as the peripheral $Mn^{II}\cdots Mn^{III}$ exchange interactions are ferromagnetic in nature. Our results are broadly in agreement with the experimental results: (i) molecules deposited on HOPG tend to retain the oxidation state but the HOMO–LUMO gap is altered significantly revealing distortions and likely alteration in the spin ground state; (ii) on the Au(111) surface where various concentrations of the $\{Mn_{19}\}$ sample on Au(111) have been studied,[12a] the XAS spectra reveal a significant enhancement of the M_l values enlightening the surface induced distortions in the geometry as specifically revealed in our calculations. Additionally, *M vs. H* data obtained from XMCD measurements reveal that the ground state *S* value of $\{Mn_{19}\}$ on Au(111) was drastically reduced (for some concentration, the reported value is $S = 5/2 \pm 0.07$ and for another $S = 7/2 \pm 0.3$). Experiments also reveal a significant number of Mn^{III} ions being reduced to

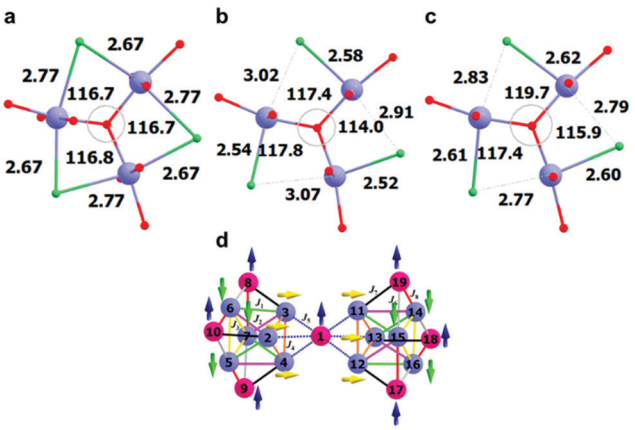

Fig. 2 Structural parameters associated with the J_3 interactions for (a) X-ray, (b) end-on and (c) side-on geometries depicting the variations observed. (d) Expected ground state electronic configuration of **1** in the end-on binding mode upon adsorption in Au(111).

isotropic Mn^{II} ions by the surface and the number of Mn^{II} ions in the cluster is found to correlate to the layer concentrations.[12a] While the Au(111) surface tends to reduce the Mn^{III} ions, deposition on the HOPG surface tends to retain the oxidation state, revealing specifics of the surface-induced reduction. Alterations in the ground state due to distortion in the geometry are likely to be the general cause on any surface and hence retaining the large spin ground state on any surface is likely to pose a challenge for this cluster.

As experimental studies on the Au(111) surface suggest that the Mn^{III} ions undergo reduction to form Mn^{II} ions which are isotropic in nature, we decided to explore theoretically the geometry of fully reduced $\{Mn^{II}_{19}SMe\}$ cluster using a model structure with a formula of $[Mn^{II}_{19}(\mu_4\text{-}O)_8(\mu_3\text{-}Cl)_8(HLSMeH)_{10}(HLSMe)_2(MeOH)_6]$ (see ESI,† Fig. S6 for the geometry). Here, we have explored the geometry of the cluster in end-on mode and the binding energy is computed to be -432.4 kJ mol^{-1} and this is significantly larger than the one computed for the unreduced complex. This reveals that the energetic cost associated with the reduction is likely to be compensated by the formation energy upon reduction. The geometry around the Mn^{III} ions is significantly altered as expected; in particular, the Jahn–Teller elongation observed for the Mn^{III} ions was lost upon reduction (see Table S5 in ESI† for selected structural parameters for comparison). Furthermore, we have also computed the energetic cost associated with the reduction by estimating the energy difference between the fully reduced and the original structure and this energy difference is estimated to be +3.5 eV per $Mn^{3+} \rightarrow Mn^{2+}$ redox pair and this is significantly large compared to the standard redox couple of the $Mn^{3+} \rightarrow Mn^{2+}$ pair and this is likely due to the role of the Au(111) surface in enhancing the reduction process.[15] As the computed energetics for the reduced state is favorable and the binding energies of the reduced species on Au(111) are higher than the unreduced complexes, these factors lead to spontaneous reduction of the Mn^{III} ions to Mn^{II} ions. These results are in agreement with XMCD and XAS measurements performed earlier using 1.5×10^{-6} M concentration of complex **1** in solution.[12a] The spin density ranging from 4.75 to 4.83 on the Mn^{II} ions establishes the oxidation state of the reduced manganese ions.

Additionally, we have also computed the magnetic exchange coupling for this fully reduced $\{Mn^{II}_{19}\}$ cluster and these results are given in Table 1. We have found that all the J values except J_1 are antiferromagnetic in nature. In particular, the J_2 interaction becomes strongly antiferromagnetic upon reduction and this is due to the subtle structural changes around the coordination sphere. Particularly the Mn^{II}–O–Mn^{II} angles are substantially larger (115° *vs.* 125° in the reduced structure) leading to a larger J. The strength of antiferromagnetic J is found to be similar for many interactions and various parameters; in particular, the Mn–O–Mn angles are found to play an important role in dictating the strength of the J values (see Table S4 in ESI†). With the estimated Js, we have also attempted to work out the ground state S value based on calculations on smaller models, this reveals a significant spin-frustration within the cluster leading to $S = 5/2$ as a possible ground state S value and this strikingly correlates with the ground state reported for the reduced $\{Mn_{19}\}$ complex on Au(111).

Our calculations unequivocally establish that there are some minor alterations on the structure upon adsorption and this drastically reduces the spin ground state by altering the corresponding magnetic coupling.[12a] Reduction of Mn^{III} to Mn^{II} is found to alter the Js from ferromagnetic to antiferromagnetic leading to a drastic reduction in the spin ground state. All these observations are in agreement with earlier experiments. Retaining the magnetic properties of SMMs on the surface is one of the holy grails in this area and our results reveal that not only the magnetic core but also the coordination environment around the metal ions also need to be protected to guard the magnetic properties from structural distortions.

GR thanks SERB (CRG/2018/000430) for funding. GR thanks IITB for the HPC facility. RN thanks IITB for the SRF fellowship.

Conflicts of interest

There are no conflicts to declare.

Notes and references

1 L. Bogani and W. Wernsdorfer, *Nat. Mater.*, 2008, **7**, 179–186.
2 E. Moreno-Pineda, C. Godfrin, F. Balestro, W. Wernsdorfer and M. Ruben, *Chem. Soc. Rev.*, 2018, **47**, 501–513.
3 (*a*) E. Coronado, A. Forment-Aliaga, F. M. Romero, V. Corradini, R. Biagi, V. De Renzi, A. Gambardella and U. del Pennino, *Inorg. Chem.*, 2005, **44**, 7693–7695; (*b*) A. Gryzia, T. Volkmann, A. Brechling, V. Hoeke, L. Schneider, K. Kuepper, T. Glaser and U. Heinzmann, *Nanoscale Res. Lett.*, 2014, **9**, 60.
4 (*a*) M. Mannini, F. Pineider, C. Danieli, F. Totti, L. Sorace, P. Sainctavit, M.-A. Arrio, E. Otero, L. Joly and J. C. Cezar, *Nature*, 2010, **468**, 417–421; (*b*) A. Caneschi, D. Gatteschi and F. Totti, *Coord. Chem. Rev.*, 2015, **289–290**, 357–378.
5 (*a*) C. A. Goodwin, F. Ortu, D. Reta, N. F. Chilton and D. P. Mills, *Nature*, 2017, **548**, 439; (*b*) F. S. Guo, B. M. Day, Y. C. Chen, M. L. Tong, A. Mansikkamäki and R. A. Layfield, *Angew. Chem., Int. Ed.*, 2017, **56**, 11445–11449; (*c*) F.-S. Guo, B. M. Day, Y.-C. Chen, M.-L. Tong, A. Mansikkamäki and R. A. Layfield, *Science*, 2018, **362**, 1400–1403.
6 M. Mannini, F. Bertani, C. Tudisco, L. Malavolti, L. Poggini, K. Misztal, D. Menozzi, A. Motta, E. Otero and P. Ohresser, *Nat. Commun.*, 2014, **5**, 4582.
7 F. Totti, G. Rajaraman, M. Iannuzzi and R. Sessoli, *J. Phys. Chem. C*, 2013, **117**, 7186–7190.
8 G. Rajaraman, A. Caneschi, D. Gatteschi and F. Totti, *J. Mater. Chem.*, 2010, **20**, 10747–10754.
9 (*a*) C. J. Milios, A. Vinslava, W. Wernsdorfer, S. Moggach, S. Parsons, S. P. Perlepes, G. Christou and E. K. Brechin, *J. Am. Chem. Soc.*, 2007, **129**, 2754–2755; (*b*) A. Cornia, A. C. Fabretti, M. Pacchioni, L. Zobbi, D. Bonacchi, A. Caneschi, D. Gatteschi, R. Biagi, U. Del Pennino and V. De Renzi, *Angew. Chem., Int. Ed.*, 2003, **42**, 1645–1648.
10 (*a*) S. Mameri, A. M. Ako, F. Yesil, M. Hibert, Y. Lan, C. E. Anson and A. K. Powell, *Eur. J. Inorg. Chem.*, 2014, 4326–4334; (*b*) S. Kang, H. Zheng, T. Liu, K. Hamachi, S. Kanegawa, K. Sugimoto, Y. Shiota, S. Hayami, M. Mito and T. Nakamura, *Nat. Commun.*, 2015, **6**, 5955; (*c*) E. Ruiz, T. Cauchy, J. Cano, R. Costa, J. Tercero and S. Alvarez, *J. Am. Chem. Soc.*, 2008, **130**, 7420–7426.
11 C.-H. Ge, Z.-H. Ni, C.-M. Liu, A.-L. Cui, D.-Q. Zhang and H.-Z. Kou, *Inorg. Chem. Commun.*, 2008, **11**, 675–677.
12 (*a*) J. Dreiser, A. M. Ako, C. Wäckerlin, J. Heidler, C. E. Anson, A. K. Powell, C. Piamonteze, F. Nolting, S. Rusponi and H. Brune, *J. Phys. Chem. C*, 2015, **119**, 3550–3555; (*b*) A. M. Ako, M. S. Alam, S. Mameri, Y. Lan, M. Hibert, M. Stocker, P. Müller, C. E. Anson and A. K. Powell, *Eur. J. Inorg. Chem.*, 2012, 4131–4140.
13 G. Rajaraman, A. Caneschi, D. Gatteschi and F. Totti, *Phys. Chem. Chem. Phys.*, 2011, **13**, 3886–3895.
14 P. Comar, T. Rajeshkumar, G. S. Nichol, M. B. Pitak, S. J. Coles, G. Rajaraman and E. K. Brechin, *Dalton Trans.*, 2015, **44**, 19805–19811.
15 M. Tamaru, P. Barpanda, Y. Yamada, S.-i. Nishimura and A. Yamada, *J. Mater. Chem.*, 2012, **22**, 24526–24529.